CO-Induced Structural Rearrangement of the C Cluster in *Carboxydothermus hydrogenoformans* CO Dehydrogenase—Evidence from Ni K-Edge X-ray Absorption Spectroscopy†

Weiwei Gu,‡,§ Javier Seravalli,|| Stephen W. Ragsdale,|| and Stephen P. Cramer*,‡,§

Physical Biosciences Division, Lawrence Berkeley National Laboratory, Berkeley, California 94720, Department of Applied Science, University of California, Davis, California 95616, and Department of Biochemistry, University of Nebraska, Lincoln, Nebraska 68588

Received November 24, 2003; Revised Manuscript Received March 26, 2004

ABSTRACT: We have examined the C cluster in type II CO dehydrogenase (CODH) from *Carboxydothermus hydrogenformans* using Ni K-edge X-ray absorption near edge spectroscopy and extended X-ray absorption fine structure (EXAFS) spectroscopy. The enzyme was studied under three conditions: "as-isolated" and after treatment with CO or Ti^{III}. The shape of the Ni K-edge changes slightly between the different conditions, but no significant edge shift is seen, suggesting that the C cluster contains Ni^{II} in both forms. The Ni EXAFS of as-isolated CODH can be simulated with 4 Ni−S interactions at 2.20 Å with a large spread in distances. A light atom (C, N, O) is not required to fit the spectrum. After CO treatment, significant changes are observed in the EXAFS. A new feature appears at ∼2.7 Å; this component is consistent with a Ni−Fe interaction. The average Ni−S distance also expands to ∼2.25 Å. The changes between the two forms suggest that the active site (C cluster) undergoes structural rearrangement after CO treatment, and the observed changes help reconcile the two different crystal structures. The implications of the structural change for the enzyme activation and mechanism are discussed.

Ni-containing carbon monoxide dehydrogenase (CODH)[1] is a key enzyme of various energy-yielding pathways in a variety of autotrophic anaerobes (*1*−*3*). This enzyme catalyzes the two-electron oxidation of CO to CO_2:

$$CO + H_2O \rightleftarrows CO_2 + 2H^+ + 2e^-$$

This reaction allows bacteria such as *Rhodospirillum rubrum* (*4*, *5*) and *Carboxydothermus hydrogenoformans* (*6*) to grow with CO as the sole carbon and energy source. It is coupled with the reduction of protons to H_2 in hydrogenogenic *C. hydrogenoformans* (*7*, *8*). CODH also combines with acetyl-CoA synthase (ACS) to fix CO_2 to acetyl-CoA in acetogens or to cleave acetyl-CoA to produce methane and CO_2 in methanogens (*2*, *3*, *9*). In this case, it generates CO as a metabolic intermediate (*10*). Apart from its key role in microbial metabolism, CODH is important for the regulation of atmospheric carbon monoxide levels. Each year, most of the 10^{12} kg of CO entering the atmosphere of the earth originate from human activities (*11*). The ability of CODH to convert CO to CO_2 or to incorporate CO into organic carbon and cell material is pivotal for the recycling of global CO (*2*).

Crystal structures of CODHs have been reported for "type II" *C. hydrogenoformans* (Ch-CODH II), *R. rubrum* (Rr-CODH), and *Moorella thermoacetica* CODH/ACS (*12*, *13*). In the first two structures, which involve monofunctional CODHs, the protein is composed of two identical subunits, which contain three Fe_4-S_4 clusters (two B clusters and one D cluster) and two Ni−Fe clusters (C clusters). The C cluster is widely accepted as the active site of CO oxidation, while the B and D clusters are thought to transfer electrons between the active site and electron acceptors interacting at the protein surface (*3*, *8*, *12*). The 1.63-Å resolution structure for Ch-CODH revealed that the C cluster is a novel Ni−Fe−S cluster, containing one Ni, four Fe, and five labile sulfur atoms (*8*). The Ni ion is incorporated in a highly distorted $NiFe_3S_4$ cubanelike cluster, coordinated by four S atoms in an approximately square planar geometry and bridged to an external Fe through an inorganic sulfide. All four Fe atoms are bridged to Ni through inorganic sulfide ligands, with Ni−Fe distances spread over nearly 1 Å (2.8, 2.9, 3.3, and 3.7 Å). In the 2.8-Å resolution structure of Rr-CODH (*12*), the Ni adopts a different geometry that could be described as distorted tetrahedral (with three S and one unidentified light atom) or trigonal bipyramidal (with four S and one light atom as ligands). The external Fe is bridged directly to the Ni by a cysteine S ligand, the prior bridging sulfide has disappeared, and the four Ni−Fe distances are clustered within a much tighter range of 2.6−2.8 Å (Chart 1) (*12*).

† This work was funded by NIH Grants GM-44380 (S.P.C.), GM-65440 (S.P.C.), and GM39451 (S.W.R.) and the DOE Office of Biological and Environmental Research (S.P.C.). SSRL is supported by the Department of Energy, Office of Basic Energy Sciences.

* To whom correspondence should be addressed. Tel: 530-752-0360. Fax: 530-752-2444. E-mail: cramer@lbl.gov.

‡ Lawrence Berkeley National Laboratory.

§ University of California.

|| University of Nebraska.

[1] Abbreviations: XANES, X-ray absorption near edge spectroscopy; EXAFS, extended X-ray absorption fine structure; CODH, CO dehydrogenase.

10.1021/bi036104e CCC: $27.50
Published on Web 06/19/2004

Chart 1: Comparison of the Two CODH Crystal Structures[a]

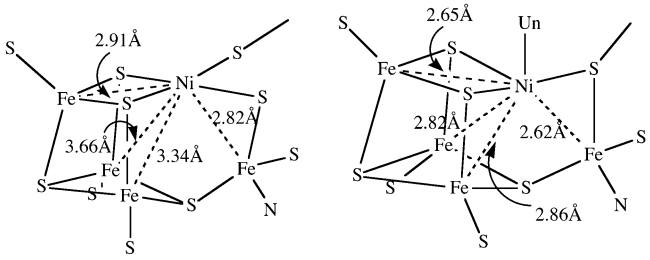

[a] Left, structure of Ch-CODH II (*8*). Right, structure of Rr-CODH (*12*). Un = unidentified light atom.

The C cluster has been studied extensively by a variety of spectroscopic methods (*14*−*21*). In previous Ni extended X-ray absorption fine structure (EXAFS) spectra for Rr-CODH (*20*), a Ni−Fe interaction was not observed, and it was proposed that Ni is coordinated by two S and two to three N/O ligands (*20*). Electron paramagnetic resonance (EPR) and Mössbauer spectroscopy on a Ni-deficient and holo enzyme suggested that the C cluster is composed of a high-spin Ni^{II} bridged to a typical $[Fe_4S_4]$ cluster (*18*). Later EPR studies found a unique ($g = 2.16$) signal (*14*), which was assigned to a [NiFe] center. This [NiFe] EPR signal is heterogeneous, but the heterogeneity can be removed by CO treatment (*17*). A model was proposed in which the Fe site in a [NiFe] cluster is bridged to the $[Fe_4S_4]$ cluster (*14*, *17*). However, a recent magnetic circular dichroism study found that the reduced Ni-deficient C cluster was distinctly different from a typical $S = {}^3/_2[Fe_4S_4]^+$ with spectra that resembled those of reduced $[Fe_3S_x]$ clusters (*15*), consistent with the recent crystallographic data.

The activity of CODH is redox-dependent (*22*, *23*). The enzyme has a very low catalytic activity for CO_2 reduction at potentials > -300 mV. The maximum activity is observed at potentials < -480 mV (*22*), for example, by incubating the as-isolated enzyme in CO. The fact that CODH can exist in both inactive and active states complicates the interpretation of previous spectroscopic studies.

In this paper, we report the Ni X-ray absorption near edge spectroscopy (XANES) and EXAFS studies for Ch-CODH in both "as-isolated" and "CO-treated" forms. Although little other spectroscopy has been done on this particular protein, genetic analysis has shown that the sequence of Ch-CODH is highly similar to the Rr-CODH and the β subunit of the *M. thermoacetica* CODH/ACS (*24*). The Ch-CODH has extremely high catalytic activity and significantly higher spin concentrations (*7*), indicating that it is more homogeneous relative to other CODHs that have been studied. Special care was taken to keep the CO-treated sample in a homogeneous CO-treated state because CO undergoes rapid oxidation by the enzyme. The data are compared with previous EXAFS and crystallography studies.

MATERIALS AND METHODS

Protein Purification and Sample Preparation. Ch-CODH II was purified and assayed in the Ragsdale lab according to the published procedures (*8*). All purification steps and sample preparations were carried out in a Vacuum Atmospheres anaerobic chamber (Hawthorne, CA) at an oxygen tension below 2 ppm. The purified CODH II had a specific CO oxidation activity of 19 500 μmol min^{-1} mg^{-1} in the as-isolated state. The protein was concentrated to a final concentration of 0.9 mM in 0.1 M Tris at pH 8.0, containing 20% glycerol for the X-ray measurements. EPR spectra were recorded with a Bruker ESP300e instrument along with an Oxford Instruments liquid He cryostat. The microwave frequency was measured with a Hewlett−Packard counter model 5352B. The total integrated spin intensity for the as-isolated CODH II at 10 K was 0.04 spins per homodimer (only B_{red} was observed). For CO-treated CODH II, the total spin intensities were 2.2 and 3.3 spins per homodimer at 25 (B_{red}) and 10 K ($C_{red2} + B_{red}$), respectively. The as-isolated Ch-CODH was loaded into an EXAFS sample holder and frozen in liquid nitrogen in an anaerobic bottle. The CO-treated sample was flushed with CO in an anaerobic bottle for 5 min and then loaded into an EXAFS sample holder in the sample bottle under CO gas using a Hamilton gastight syringe. The bottle was then frozen and stored in liquid nitrogen until the X-ray absorption spectroscopy measurements. The Ti^{3+}-reduced sample was prepared by adding 2.5 mM Ti^{3+}−citrate to the enzyme.

X-ray Absorption Measurements. Ni K-edge X-ray absorption spectra were recorded using Si(220) monochromator crystals at beamlines 7-3 and 9-3 at the Stanford Synchrotron Radiation Laboratory (SSRL). The energy was calibrated using a Ni foil as an internal standard in a three ion-chamber geometry, using 8331.6 eV as the first inflection point of the Ni-foil spectrum. All ion chambers were filled with N_2. Harmonic rejection at beamline 7-3 was accomplished by detuning the second monochromator crystal to 50% of maximum possible flux. At beamline 9-3, the crystal was fully tuned and a harmonic rejection mirror with energy cut off at 11 keV was used. During all X-ray measurements, the samples were maintained at ~10 K using an Oxford Instruments CF1208 helium-flow cryostat. To reduce radiation damage, the enzyme samples were moved to a different position after every fourth scan. The Ni K-edge energy of the enzyme was monitored on sequential scans to confirm the integrity of the enzyme in the X-ray beam.

Ni EXAFS spectra were recorded to $k = 12.5$ Å^{-1} in 25-min scans (12−18 scans per sample). Fluorescence excitation spectra were collected using a Canberra 30-element Ge detector and Canberra 2026 amplifiers with 0.125-μs shaping times. Single-channel analyzers were used to set an electronic window on the Ni Kα fluorescence. The average Ni signal count rate at each individual detector element was ~6000 cps, while the total count rates were on the order of 80 000 cps at the end of each scan.

XANES Analysis. The preedge features were isolated after subtracting an arctangent function that fit the overall edge. The isolated transitions were fitted by two Gaussian components centered at 8332 and 8336 eV, respectively. The normalized intensities for "1s → 3d" and "1s → $4p_z$" transitions were obtained by integrating these Gaussian components centered at 8332 and 8336 eV, respectively.

EXAFS Data Analysis. The EXAFS oscillations were extracted from the averaged spectra using the EXAFSPAK analysis software (*25*), using 8350 eV as an initial E_0 for defining the photoelectron wave vector. The resultant EXAFS data were weighted by k^3 over the region $k = 1-12.5$ Å^{-1}. Least-square fits of the EXAFS data were performed using Fourier-filtered data, using the following approximate for-

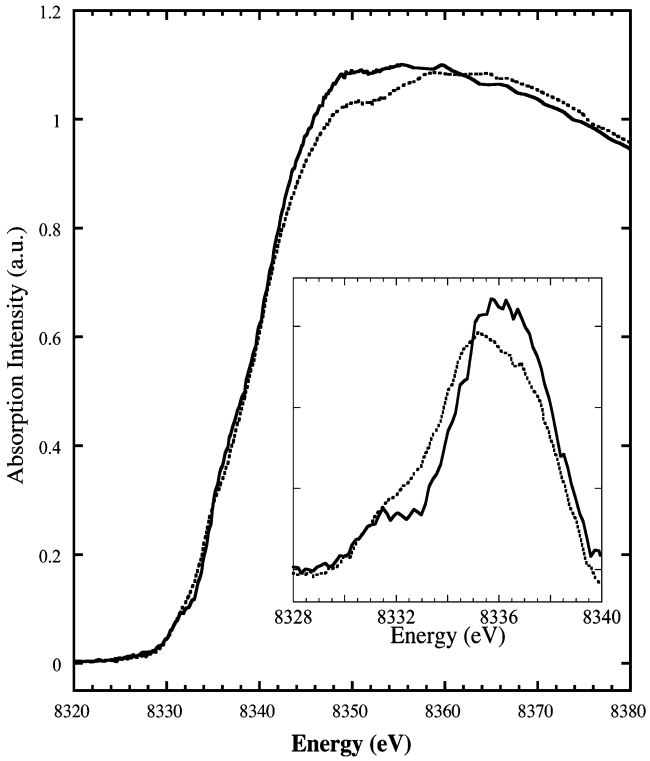

FIGURE 1: Ni K-edge XANES of as-isolated (—) and CO-treated (- - -) Ch-CODH II. (Insert) Features obtained after subtracting an arctangent function that fit the overall edge.

mula to optimize the structural parameters N_b, R_{ab}, and σ_{ab}^2:

$$\chi(k) = S_0^2(k)\sum_b \frac{N_b}{kR_{ab}^2}|f_b(k)|\, e^{-2\sigma_{ab}^2 k^2}\, e^{-[2R_{ab}/\lambda(k)]} \times \sin[2kR_{ab} + \phi_{ab}(k)]$$

In this equation, N_b is the number of backscatterers in the *b*th backscattering shell at distance R_{ab} from the X-ray absorber, $f_b(k)$ and $\phi_{ab}(k)$ are the backscattering amplitude and total phase-shift of the absorber−scatterer pairs, respectively, σ_{ab}^2 is the mean square deviation of R_{ab}, and $\lambda(k)$ represents the mean free path of the ejected photoelectron. S_0^2(k) is an amplitude reduction factor that accounts for multiple-electron excitations and was fixed at 0.9 during the fitting process. The functions $f_b(k)$, $\phi_{ab}(k)$, and $\lambda(k)$ were calculated using FEFF 7.01 (*26*). The goodness of fit was determined by

$$F = \sum_i [\chi(k_i)_{calc} - \chi(k_i)_{obs}]^2 k^6$$

RESULTS

XANES Analysis. Ni K-edge spectra for as-isolated and CO-treated Ch-CODH samples are shown in Figure 1. The overall shape of the as-isolated spectrum is very similar to the previously reported Ni K-edge for Rr-CODH (20). A preedge transition at ~8332 eV and a poorly resolved shoulder at 8336 eV are observed. These features are assigned to the "1s → 3d" and "1s → $4p_z$" transitions, respectively (*27*, *28*). The normalized integrated intensity of the 8332 peak (0.079 eV) suggests 4- or 5-coordinate Ni (*28*). The edge inflection point energy (8340 eV) is consistent with Ni^{II} (*29*−*32*).

There is no overall edge energy shift between the as-isolated and CO-treated forms, indicating that the average Ni oxidation state is the same in both samples. However, the shape of the XANES spectra does change after CO treatment. The integrated "1s → 3d" transition intensity increases to 0.099 eV in the CO-treated form, while the "1s → $4p_z$" transition becomes less distinct (Figure 1). The strength of both of these features is strongly related to the metal geometry. For noncentrosymmetric geometries, such as tetrahedral, the dipole forbidden "1s → 3d" transition gains intensity by p−d mixing (*27*). Thus, this feature is strongest in a tetrahedral geometry and weakest in square planar or octahedral geometries. The increase of the "1s → 3d" transition in the CO-treated form and the diminished resolution of the "1s → $4p_z$" feature are consistent with Ni moving away from a square planar geometry.

Differences are also observed in the XANES at higher energies. The CO-treated enzyme spectrum has a more obvious shoulder (but less intensity) near 8350 eV, while this spectrum has somewhat more intensity after 8362 eV. The structure of the XANES in this region depends in a complex manner on the multiple scattering of the outgoing photoelectron (*33*); we do not have a unique interpretation for these changes. We simply note that the XANES spectra indicate that, upon CO treatment, the Ni ion remains in the Ni^{II} oxidation state and adopts a different, less "centrosymmetric" geometry.

EXAFS Spectra. The *k*-space EXAFS and Fourier transform (FT) for the as-isolated, CO-treated, and Ti^{III}-reduced samples are shown in Figure 2. For the as-isolated CODH, there is only one significant peak in the FT spectrum. This peak can be fit by four Ni−S interactions at ~2.20 Å. However, the Debye−Waller factor (σ = 0.08 Å) for the Ni−S shell is much higher than that for typical Ni−S interactions (*32*). Studies of Ni model systems found that the vibrational contribution (σ_{vib}) to bond length disorder σ is on the order of 0.05 Å for Ni−S interactions at 2.20 Å (*32*, *34*). The larger σ obtained for as-isolated CODH indicates that the Ni−S shell is structurally disordered; because the contributions add in quadrature, an approximate value for the static disorder (σ_{stat}) is ~0.06 Å. The fit with a slightly disordered Ni−S shell is adequate, and neither a shorter distance Ni−N/O component nor longer distance Ni−Fe contributions are required to simulate the data.

For the CO-treated form of Ch-CODH, the strong Ni−S peak remains, but the average Ni−S distance increases to 2.25 Å (Figure 2 and Table 1). Ni−S distances can be an indicator of Ni geometry (*32*). The longer bond length indicates either that the Ni site is more reduced in the CO-treated form or that the Ni geometry and/or coordination number changes. Because the Ni K-edge shows no obvious energy shift, the first alternative can be excluded. For 4-coordinate Ni compounds, the average Ni−S distances range from 2.10 to 2.24 Å for approximately square planar complexes and from 2.27 to 2.31 Å for tetrahedral complexes (*32*). For 5-coordinate complexes, an average Ni−S bond length of 2.29 Å was observed. The observed Ni−S distance of 2.25 Å falls between the values seen for strictly square planar and tetrahedral geometries, and neither extreme appears likely. However, the increased Ni−S bond length is

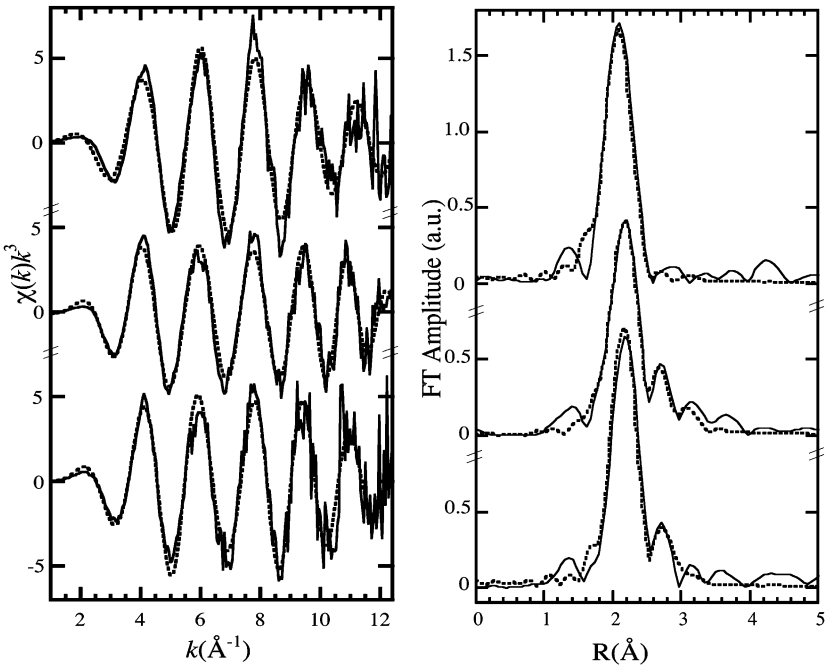

FIGURE 2: (Left) Ni EXAFS (—) and best fits (- - -) for as-isolated (top), Ti^{3+}-reduced (middle), and CO-treated (bottom) Ch-CODH II. (Right) Ni EXAFS FTs (—) and transforms of best fits (- - -) as described in the left panel. The transforms were phase-shifted corrected using a Ni−S phase shift.

Table 1: Summary of Curve-Fitting Analyses of Ch-CODH II Ni EXAFS under Different Conditions

sample	*N*	type	*R* (Å)	*σ* (Å)	*F*
as-isolated Ch CODH	4	S	2.201(4)	0.083	242.9
CO-treated Ch CODH	4	S	2.247(4)	0.088	221.6
	4	S	2.252(3)	0.088	143.0
	1	Fe	2.744(5)	0.082	
	4	S	2.248(3)	0.087	142.2
	1	Fe	2.741(5)	0.0083	
	1	C	1.801(43)	0.147	
	4	S	2.252(3)	0.088	134.7
	1	Fe	2.744(5)	0.083	
	0.3	C	1.717(16)	0.050	
Ti^{3+}-reduced Ch CODH	4	S	2.245(4)	0.080	419.0
	4	S	2.249(4)	0.080	357.2
	1	Fe	2.749(9)	0.092	

at least consistent with the conclusion from the preedge transitions that the Ni site changes geometry in the CO-reduced state.

A new feature at ~2.7 Å appears in the EXAFS FT for the CO-treated enzyme, and this component can be simulated by one Ni−Fe interaction at 2.74 Å, with a σ of 0.08 Å (larger Ni−Fe coordination numbers would require larger σ values). The distance (2.74 Å) is shorter than the X-ray diffraction results for Ch-CODH II, where the shortest Ni−Fe distance is at 2.82 Å and the overall average Ni−Fe distance is >3 Å (Chart 1) (*8*). In the Drennan Rr-CODH structure, the average Ni−Fe distance is in fact the same 2.74 Å that we report, but the individual values range from 2.62 to 2.86 Å.

Because there is little doubt that four Fe atoms are always in reasonable proximity to the C cluster Ni in CODH, the missing Fe in the as-isolated EXAFS spectra needs to be explained, as well as the still weak signal in the CO-treated EXAFS. For the as-isolated C cluster, the likely answer is that because of the wide range of Ni−Fe distances, varying from 2.8 to 3.7 Å (*8*), destructive interference between different Ni−Fe components cancels out the EXAFS signal. This phenomenon can be illustrated by one simulation (out of many) (Figure 3), which shows an overall EXAFS spectrum with two Ni−Fe interactions at different distances (2.7 and 2.9 Å). Other EXAFS parameters were fixed according to the experimental values obtained from the spectra of the CO-treated sample. The *k*-space spectra for the two Ni−Fe components show EXAFS oscillations that are π out of phase in the middle of the spectrum, where the individual amplitudes are largest. Therefore, most contributions from the Ni−Fe interactions cancel each other, and the resulting EXAFS FT spectrum looks very similar to that for the as-isolated Ch-CODH (Figures 2 and 3). Fortuitous cancellation of the overlapping components is not an uncommon problem for EXAFS analyses.

On the basis of radioactive-labeling experiments, CO was proposed to be an internal ligand for the C cluster (*23*), and the Rr-CODH crystal X-ray diffraction analysis also suggested that Ni binds a CO or other diatomic ligand (*12*). For our CO-treated Ch-CODH II, a possible Ni−C interaction was investigated; however, adding a one Ni−C interaction to the fit does not result in a significant improvement in the fit quality, and the required σ value is unreasonable (Table 1). In fits constrained to a reasonable σ of 0.05 Å, the largest estimate for the Ni−C coordination number was 0.3. Although CO treatment has clearly modified the properties of the Ch-CODH II Ni site, it is clear that we have not trapped a form with a significant fraction of CO bound to Ni. A similar EXAFS spectrum is observed for the enzyme form, which is reduced by Ti^{3+}−citrate (Figure 2 and Table 1), supporting the hypothesis that CO treatment of an oxidized enzyme only results in the reduction of the C cluster without the binding of CO to the Ni center.

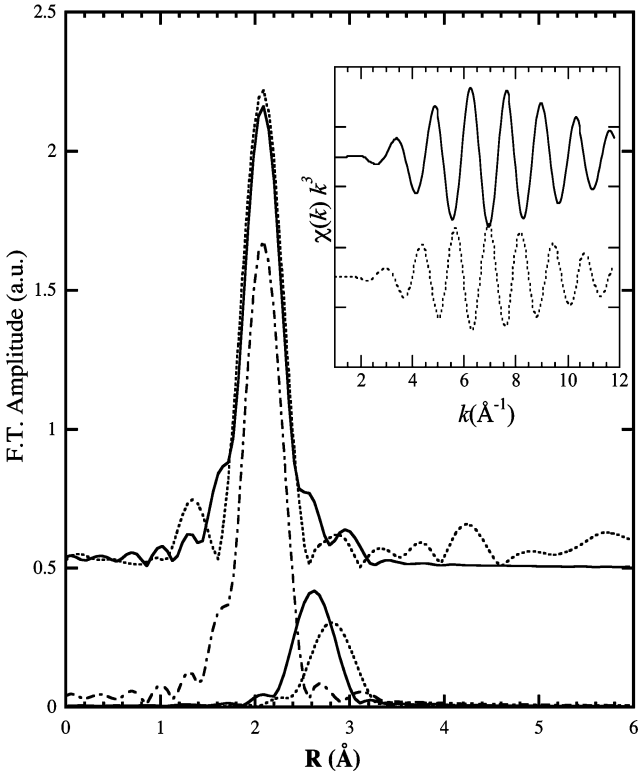

FIGURE 3: (Top) Calculated Ni EXAFS FT (—) for a system with four Ni−S interactions at 2.2 Å, one Ni−Fe at 2.7 Å, and one Ni−Fe at 2.9 Å and the spectrum for the as-isolated protein (- - -). The Debye−Waller factors (σ^2) for the two Ni−Fe interactions were 0.007 and 0.008 Å^2, respectively. (Bottom) Individual EXAFS component for Ni−S at 2.2 Å (-•-•-), Ni−Fe at 2.7 Å (—), and Ni−Fe at 2.9 Å (- - -). (Insert) Individual EXAFS component in *k* space for Ni−Fe interactions at 2.7 (—) and 2.9 Å (- - -).

DISCUSSION AND CONCLUSIONS

The results from our Ch-CODH XAFS experiments have the potential to resolve some of the apparent discrepancies that have accumulated among different spectroscopic and crystallographic studies of the C cluster, some of which have been noted in a recent review (*35*). Although the possibility of a $NiFe_3S_4$ cubane structure for the C cluster was noted early on, a regular cubane structure was ruled out by previous EXAFS studies (*20*) (The authors noted that longer distance Ni−Fe interactions might not be observed). Thus, the presence of a $NiFe_3S_4$ core (as well as an external Fe) came as something of a surprise when the first two crystal structures were reported. Upon closer inspection, however, we observe wide disparities in the different Ni−Fe distances in the Ch-CODH structure (Chart 1); therefore, it is not unexpected that these interactions are not clearly observed in the EXAFS. In fact, Tan noted that a fractional 2.7-Å Ni−Fe interaction could be accommodated in certain individual data sets (*36*).

The current EXAFS results also address apparent discrepancies between the two crystallographic studies on monofunctional CODH C clusters. When the two clusters are superimposed (Figure 4), there are two major differences. First, the μ_2-S, which bridges Ni and the external Fe in the Ch-CODH II structure, is not seen with Rr-CODH; instead, a cysteine S bridges these two metal ions. Second, in the Ch-CODH II structure, Ni is farther away from the center of the Fe_3 subcluster, resulting in Ni−Fe distances distributed

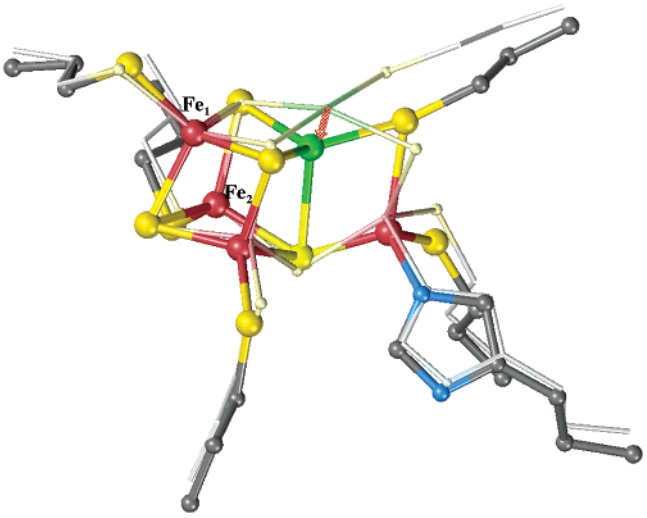

FIGURE 4: Comparison of the two crystal structures for Ch-CODH II (*8*) (dark color and ball-and-stick model) and Rr-CODH (*12*) (light color and stick model). The structure was aligned using DS ViewerPro 5 (*42*) by first defining Fe_1 and Fe_2 as two tethers. Color coding is Ni = green, Fe = red, S = yellow, C = black, and N = blue.

from 2.8 to 3.7 Å. In contrast, in the Rr-CODH, the Ni is almost completely integrated into the cluster and the Ni−Fe distances range from 2.6 to 2.8 Å. According to the reported experimental procedures, the CODH crystals were grown under different conditions; Ch-CODH II was crystallized in the presence of dithionite, while Rr-CODH was crystallized from a CO-treated solution (*8*, *12*). The activity of CODH is markedly sensitive to its initial redox potential, and incubation with CO has been shown to promote an "autocatalytic" activation of the enzyme (*22*). Our results support the interpretation that the absence or presence of CO, which is a potent electron donor for CODH, in the buffer (and not crystallographic resolution) is the main source of the structural differences.

The proposed catalytic mechanisms for CO oxidation by CODH involve the binding of CO and hydroxide to metals and subsequent nucleophilic attack on the metal−CO by a metal-bound OH group (*3*, *8*, *12*). Interpreting the Drennan structure as the active form of the C cluster is thus satisfying because it brings the Ni and external Fe closer together. The question remains; what is the driving force for the structural transformation that also produces catalytic activity?

It has been shown that activation of CODH can be achieved *either* with CO or with low redox potentials (following the Nernst equation as a 1-electron process with a midpoint potential of −316 mV) (*17*, *22*, *23*). Thus, the CO molecule itself is not required, merely a low-potential electron. Redox-dependent conformational changes in Fe−S clusters are well-documented; two examples are the $[Fe_4S_4]$ cluster of the nitrogenase Fe protein (*37*) and the P cluster of the nitrogenase MoFe protein (*38*, *39*). At very low redox potentials, two of the Fe−Fe distances in the $[Fe_4S_4]$ cluster for the nitrogenase Fe protein decrease from 2.75 to 2.53 Å (*37*). Two other cases that appear especially relevant are the reductive activations of Ni−Fe hydrogenase (*40*) and aconitase (*41*).

In summary, XANES and EXAFS spectra provide evidence for a redox-dependent structural change in the $NiFe_4S_x$ C cluster. These results support other data that have been

obtained by X-ray crystallography and biochemical assays. Analogies may exist with other known metalloproteins, but additional work is needed to test these speculations. X-ray diffraction of C-cluster crystals in spectroscopically defined states would certainly be one of these experiments.

ACKNOWLEDGMENT

We thank the SSRL biotechnology staff for their support of beamlines 7-3 and 9-3.

NOTED ADDED IN PROOF

While this paper was at the galley stage, a new crystallographic study of the Ch-CODH was reported (*43*). The authors propose that long-term CO exposure inactivates CODH. Our conclusions about structural changes upon short-term exposure remain unchanged.

REFERENCES

1. Bonam, D., and Ludden, P. W. (1987) Purification and characterization of carbon monoxide dehydrogenase, a nickel, zinc, iron−sulfur protein, from *Rhodospirillum rubrum*, *J. Biol. Chem. 262*, 2980−2987.
2. Ferry, J. G. (1995) CO Dehydrogenase, *Annu. Rev. Microbiol. 49*, 305−333.
3. Ragsdale, S. W., and Kumar, M. (1996) Nickel-Containing Carbon Monoxide Dehydrogenase/Acetyl-CoA Synthase, *Chem. Rev. 96*, 2515−2539.
4. Kerby, R. L., Ludden, P. W., and Roberts, G. P. (1995) Carbon monoxide-dependent growth of *Rhodospirillum rubrum*, *J. Bacteriol. 177*, 2241−2244.
5. Bonam, D., Lehman, L., Roberts, G. P., and Ludden, P. W. (1989) Regulation of carbon monoxide dehydrogenase and hydrogenase in *Rhodospirillum rubrum*: Effects of carbon monoxide and oxygen on synthesis and activity, *J. Bacteriol. 171*, 3102−3107.
6. Svetlichny, V. A., Sokolova, T. G., Gerhardt, M., Ringpfeil, M., Kostrikina, N. A., and Zavarzin, G. A. (1991) *Carboxydothermus hydrogenoformans* gen. nov., sp. nov., a CO-utilizing thermophilic anaerobic bacterium from hydrothermal environments of Kunashir island, *Syst. Appl. Microbiol. 14*, 254−260.
7. Svetlitchnyi, V., Peschel, C., Acker, G., and Meyer, O. (2001) Two membrane-associated NiFeS−carbon monoxide dehydrogenases from the anaerobic carbon-monoxide-utilizing eubacterium *Carboxydothermus hydrogenoformans*, *J. Bacteriol. 183*, 5134−5144.
8. Dobbek, H., Svetlitchnyi, V., Gremer, L., Huber, R., and Meyer, O. (2001) Crystal Structure of a Carbon Monoxide Dehydrogenase Reveals a [Ni−4Fe−5S] Cluster, *Science 293*, 1281−1285.
9. Terlesky, K. C., Nelson, M. J. K., and Ferry, J. G. (1986) Isolation of an enzyme complex with carbon monoxide dehydrogenase activity containing corrinoid and nickel from acetate-grown *Methanosarcina thermophila*, *J. Bacteriol. 168*, 1053−1058.
10. Menon, S., and Ragsdale, S. W. (1996) Evidence that carbon monoxide is an obligatory intermediate in anaerobic acetyl-CoA synthesis, *Biochemistry 35*, 12119−12125.
11. Khalil, M. A. K., and Rasmussen, R. A. (1984) Carbon monoxide in the earth's atmosphere: increasing trend, *Science 224*, 54−56.
12. Drennan, C. L., Heo, J.-Y., Sintchak, M. D., Schreiter, E., and Ludden, P. W. (2001) Life on carbon monoxide: X-ray structure of *Rhodospirillum rubrum* Ni−Fe−S carbon monoxide dehydrogenase, *Proc. Natl. Acad. Sci. U.S.A. 98*, 11973−11978.
13. Doukov, T. I., Iverson, T. M., Seravelli, J., Ragsdale, S. W., and Drennan, C. L. (2002) A Ni−Fe−Cu Center in a Bifunctional Carbon Monoxide Dehydrogenase/Acetyl-CoA Synthase, *Science 298*, 567−572.
14. Staples, C. R., Heo, J., Spangler, N. J., Kerby, R. L., Roberts, G. P., and Ludden, P. W. (1999) *Rhodospirillum rubrum* CO-dehydrogenase. Part 1. Spectroscopic studies of CODH variant C531A indicate the presence of a binuclear [FeNi] cluster, *J. Am. Chem. Soc. 121*, 11034−11044.
15. Craft, J. L., Ludden, P. W., and Brunold, T. C. (2002) Spectroscopic studies of nickel-deficient carbon monoxide dehydrogenase from *Rhodospirillum rubrum*: Nature of the iron−sulfur clusters, *Biochemistry 41*, 1681−1688.
16. Anderson, M. E., and Lindahl, P. A. (1996) Spectroscopic States of the CO Oxidation CO_2 Reduction Active Site of Carbon Monoxide Dehydrogenase and Mechanistic Implications, *Biochemistry 35*, 8371−8380.
17. Heo, J., Staples, C. R., Telser, J., and Ludden, P. W. (1999) *Rhodospirillum rubrum* CO-Dehydogenase. Part 2. Spectroscopic Investigation and Assignment of Spin−Spin Coupling Signals, *J. Am. Chem. Soc. 121*, 11045−11057.
18. Hu, Z. G., Spangler, N. J., Anderson, M. E., Xia, J. Q., Ludden, P. W., Lindahl, P. A., and Münck, E. (1996) Nature of the C-Cluster in Ni-Containing Carbon Monoxide Dehydrogenases, *J. Am. Chem. Soc. 118*, 830−845.
19. Ralston, C. Y., Wang, H., Ragsdale, S. W., Kumar, M., Spangler, N. J., Ludden, P. W., Gu, W., Jones, R. M., Patil, D. S., and Cramer, S. P. (2000) Characterization of Heterogeneous Nickel Sites in CO Dehydrogenases from *Clostridium thermoaceticum* and *Rhodospirillum rubrum* by Nickel L-Edge X-ray Spectroscopy, *J. Am. Chem. Soc. 122*, 10553−10560.
20. Tan, G. O., Ensign, S. A., Ciurli, S., Scott, M. J., Hedman, B., Holm, R. H., Ludden, P. W., Korsun, Z. R., Stephens, P. J., and Hodgson, K. O. (1992) On the Structure of the Nickel Iron Sulfur Center of the Carbon Monoxide Dehydrogenase from *Rhodospirillum rubrum*—An X-ray Absorption Spectroscopy Study, *Proc. Natl. Acad. Sci. U.S.A. 89*, 4427−4431.
21. DeRose, V. J., Telser, J., Anderson, M. E., Lindahl, P. A., and Hoffman, B. M. (1998) A Multinuclear ENDOR Study of the C-Cluster in CO dehydrogenase from *Clostridium thermoaceticum*: Evidence for H_xO and Histidine Coordination to the $[Fe_4S_4]$ Center, *J. Am. Chem. Soc. 120*, 8767−8776.
22. Heo, J., Halbleib, C. M., and Ludden, P. W. (2001) Redox-dependent activation of CO dehydrogenase from *Rhodospirillum rubrum*, *Proc. Natl. Acad. Sci. U.S.A. 98*, 7690−7693.
23. Heo, J., Staples, C. R., Halbleib, C. M., and Ludden, P. W. (2000) Evidence for a Ligand CO that is Required for Catalytic Activity of CO Dehydrogenase from *Rhodospirillum rubrum*, *Biochemistry 39*, 7956−7963.
24. Gonzalez, J. M., and Robb, F. T. (2000) Genetic analysis of *Carboxydothermus hydrogenoformans* carbon monoxide dehydrogenase genes cooF and cooS, *FEMS Microbiol. Lett. 191*, 243−247.
25. George, G. N., George, S. J., and Pickering, I. J. (1998) Stanford Synchrotron Radiation Laboratory, Stanford, CA.
26. Ankudinov, A. L., and Rehr, J. J. (1997) Relativistic calculations of spin-dependent X-ray-absorption spectra, *Phys. Rev. B: Condens. Matter 56*, R1712−R1715.
27. Eidsness, M. K., Sullivan, R. J., and Scott, R. J. (1988) in *The Bioinorganic Chemistry of Nickel* (Lancaster Jr., J. R., Ed.) pp 73−91, VCH Publishers, New York, NY.
28. Bagyinka, C., Whitehead, J. P., and Maroney, M. J. (1993) An X-ray Absorption Spectroscopic Study of Nickel Redox Chemistry In Hydrogenase, *J. Am. Chem. Soc. 115*, 3576−3585.
29. Colpas, G. J., Maroney, M. J., Bagyinka, C., Kumar, M., Willis, W. S., Suib, S. L., Baidya, N., and Mascharak, P. K. (1991) X-ray Spectroscopic Studies of Nickel Complexes, with Application to the Structure of Nickel Sites in Hydrogenases, *Inorg. Chem. 30*, 920−928.
30. Smith, M. C., Barclay, J. E., Cramer, S. P., Davies, S. C., Gu, W.-W., Hughes, D. L., Longhurst, S., and Evans, D. J. (2002) Nickel−iron−sulfur complexes: approaching structural analogues of the active sites of NiFe-hydrogenase and carbon monoxide dehydrogenase/acetyl-CoA synthase, *J. Chem. Soc., Dalton Trans.* 2641−2647.
31. Mandimutsira, B. S., Yamarik, J. L., Brunold, T. C., Gu, W., Cramer, S. P., and Riordan, C. G. (2001) Dioxygen Activation by a Nickel Thioether Complex: Characterization of a $Ni^{III}_2(\mu\text{-}O)_2$ Core, *J. Am. Chem. Soc. 123*, 9194−9195.
32. Gu, W., Jacquamet, L., Patil, D. S., Wang, H.-X., Evans, D. J., Smith, M. C., Millar, M., Koch, S., Eichhorn, D. M., Latimer, M., and Cramer, S. P. (2003) Refinement of the Nickel Site Structure in *Desulfovibrio gigas* Hydrogenase Using Range-Extended EXAFS Spectroscopy, *J. Inorg. Biochem. 93*, 41−51.
33. Rehr, J. J., and Albers, R. C. (2000) Theoretical approaches to X-ray absorption fine structure, *Rev. Mod. Phys. 72*, 621−654.
34. Maroney, M. J., Colpas, G. J., Bagyinka, C., Baidya, N., and Mascharak, P. K. (1991) EXAFS Investigations of the Ni Site in

Thiocapsa roseopersicina Hydrogenase—Evidence For A Novel Ni, Fe, S Cluster, *J. Am. Chem. Soc. 113*, 3962−3972.
35. Lindahl, P. A. (2002) The Ni-Containing Carbon Monoxide Family: Light at the End of the Tunnel? *Biochemistry 41*, 2097−2105.
36. Tan, G. O. (1993) in *Department of Chemistry*, Stanford University, Stanford, CA.
37. Musgrave, K. B., Angove, H. C., Burgess, B. K., Hedman, B., and Hodgson, K. O. (1998) All-Ferrous Titanium(III) Citrate Reduced Fe Protein of Nitrogenase: An XAS Study of Electronic and Metrical Structure, *J. Am. Chem. Soc. 120*, 5325−5326.
38. Christiansen, J., Tittsworth, R. C., Hales, B. J., and Cramer, S. P. (1995) Fe and Mo EXAFS of *Azotobacter vinelandii* Nitrogenase in Partially Oxidized and Singly Reduced Forms, *J. Am. Chem. Soc. 117*, 10017−10024.
39. Peters, J. W., Stowell, M. H. B., Soltis, S. M., Finnegan, M. G., Johnson, M. K., and Rees, D. C. (1997) Redox-dependent structural changes in the nitrogenase P-cluster, *Biochemistry 36*, 1181−1187.
40. Frey, M. (2002) Hydrogenases: Hydrogen-Activating Enzymes, *ChemBioChem 3*, 153−160.
41. Beinert, H., Kennedy, M. C., and Stout, D. (1996) *Chem. Rev. 96*, 2335−2373.
42. DiscoveryStudio (2002), Accelrys Inc., San Diego, CA.
43. Dobbek, H., Svetlitchnyi, V., Liss, J., and Meyer, O. (2004) Carbon monoxide induced decomposition of the active site [Ni-4Fe-5S] cluster of CO dehydrogenase, *J. Am. Chem. Soc. 126*, 5382−5387.

BI036104E